

# Design of a Long Linear Helical Subarray for High-Power Cylindrical Conformal Array Antenna

Jian-Qiong Zhang, Pengyou Huang\*, Xiang-Qiang Li, and Qingfeng Wang

**Abstract**—A Ku-band long linear helical subarray (LLHS) for a high-power cylindrical conformal array antenna has been developed. The LLHS consists of 80 helical antennas can be used to constitute conformal array of cylindrical surface. Through the research on the embedded probe structure, the adjustment of the coupling ability of different types of unit probes, the sealing method of the whole feeding, the problems of large feed reflection, and the uneven coupling amount of the unit probe in the rectangular waveguide system are solved, and the LLHS which can be used in the high-power conformal array is realized. The LLHS which is  $52.35\lambda$  length can obtain 25.2 dB gain, 2.31 dB axis ratio, 90% aperture efficiency,  $-15.65$  dB reflection at 12.5 GHz, and the reflection is lower than  $-14$  dB during 12–13 dB. In addition, it could handle a pulse power of 166 MW under vacuum condition.

## 1. INTRODUCTION

High-power microwave (HPM) antenna is the terminal of an HPM system which works from 300 MHz to 300 GHz and has a power capacity higher than 100 MW [1, 2]. Because of its function of focusing microwave generated by microwave source and radiating for specific target, its performance largely determines the overall working characteristics and application of HPM system. So far, a large number of scholars have proposed various forms of HPM antennas [3–6]. Among them, due to its high power capacity, low profile, circular polarization, and rotating-based phase shift, array antenna [7–9] has become an important research direction for HPM antennas. The high-power elements, such as helices [8, 9], slots [10], and horns [11], are used for research. On the other hand, the conformal array antenna [12–16] has become an important direction of antenna research due to its low profile, good concealment, and strong platform adaptability. The use of high-power conformal technology helps to further improve its anti-jamming capability and electronic countermeasure capability under the premise of not affecting the performance of the vehicle itself under the application environment of airborne and bomb load which is of great significance to the development of the entire high power microwave system.

However, there are few reports of high-power conformal arrays at this stage. Common conformal [12–16] antenna forms such as microstrip patches and SIW antennas [17–21] are difficult to adapt to the requirements of high power capacity due to the existence of their dielectric structure. The existing research on high-power array antennas is mainly focused on planar arrays, which size is difficult to meet the needs of high-power conformal arrays. The existing studies have shown that when performing cylindrical conformal arrays, single-column array structures can be spliced. The principle is shown in Figure 1. However, this method of achieving cylindrical conformation usually requires the width of the array to be within one wavelength, and the research on such high-power line arrays is still lacking.

This paper presents a Ku-band 80-element long linear Helical subarray (LLHS) that can be used for High-Power cylindrical conformal arrays. The width of this LLHS is within 0.6 wavelengths, which can be well adapted to cylindrical conformal arrays. The concept and architecture of the LLHS are

---

*Received 13 April 2020, Accepted 23 June 2020, Scheduled 20 October 2020*

\* Corresponding author: Pengyou Huang (1031847534@qq.com).

The authors are with the School of Physical Science and Technology, Southwest Jiaotong University, Chengdu, China.

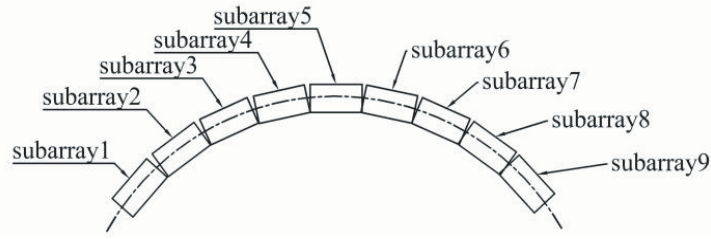


**Figure 1.** Cylindrical array synthesis schematic.

given in Section 2. The design for each component of the LLHS is presented in Section 3 and followed by the simulated power capacity performance. Section 4 tests the overall structure of the LLHS and compares it with simulation.

## 2. CONCEPT AND ARCHITECTURE

The LLHS consists mainly of a rectangular waveguide, a waveguide-coaxial adapter, a few feed probes, and some helical elements. Fig. 2 shows the overall structure of the antenna. In order to reduce the subarray spacing when forming a conformal array, the LLHS uses a rectangular waveguide with a waveguide size of  $13.6\text{ mm} \times 9\text{ mm}$  ( $0.57\lambda \times 0.375\lambda$ ) for feeding. The energy of the feed system is fed from side of the waveguide and transferred to the end waveguide-coaxial adapter sealing structure. At the same time, during the transmission process, feed probes arranged in sequence inside the rectangular waveguide couple part of the energy to the radiation element. In addition, the excitation amplitude of the element can be adjusted by optimizing the corresponding probe. The axial-mode short helical antenna [14] is chosen to be antenna element. By rotating the phase of the element helical antenna, the phase difference of the probe can be compensated, thereby improving the overall directivity of the antenna. At the same time, because the unit used is circularly polarized, the entire array is also circularly polarized. The waveguide-coaxial adapter is used for terminal coupling, so that the antenna works in the traveling wave mode, and the local field strength concentration due to standing waves is reduced.

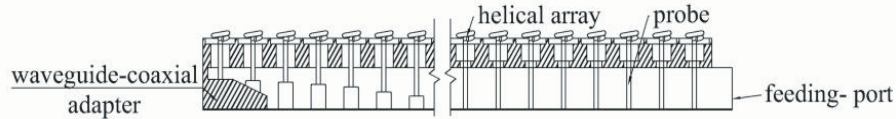


**Figure 2.** Structure of the LLHA.

The structure of the helical antenna is shown in Fig. 3. It consists of two independent helices, between which there is a relative rotation angle to adjust the phase difference, then the radiation path is divided into two. Specific evaluation to the mutual coupling is required. First, a tentative simulation is carried out to evaluate the array characteristics using closely placed DBHAs of [22], and the layout is shown in Fig. 4. This five-element array is arranged in a straight line; the elements are on random orientations, but corresponding phase compensations will be set by the input ports. The simulation results at 12.5 GHz are illustrated in Table 1. It can be seen that  $S_{11}$  increases from  $-28\text{ dB}$  to  $-18\text{ dB}$ , and the maximum  $E$ -field value soars from 9934 to 12024 V/m. During array formation, the mutual coupling between the antennas has an impact on the antenna performance, but compared to the rectangular grid array, the impact is small and can be basically ignored.

## 3. DESIGN OF THE LLHS

The key work of the LLHS is the design of the feed system. And the large difference in the unit probe coupling requirements and the difficulty in controlling the reflection coefficient of the feed system caused



**Figure 3.** Structure of the dual-branch helical antenna.



**Figure 4.** Layout of the five-element array.

**Table 1.** Results for describing the mutual coupling.

	Maximum $E$ -field	$S_{11}$
single antenna	9934 V/m	-28 dB
5-element array	12024 V/m	-18 dB

by the narrow waveguide structure become the main difficulties in its design. On the one hand, because the layout of the unit antenna is arranged in a single-row 80-unit layout, the electromagnetic energy at the feed position is relatively ample, leading to that the probe in the front should have a strong coupling suppression, while the electromagnetic energy in the terminal section is relatively scarce, so the probe in the rear section should have strong electromagnetic capability. On the other hand, due to the feed structure of the narrow waveguide, the reflection of the influence of the probe on the feed system is farther away than the previous radial-line form. The unsuitable sealing structure will also have a negative impact on the reflection coefficient and power capacity of the feed system. For this reason, the probe form of the feed system needs to be researched, and some new kinds of probes and sealing method are adopted to solve the problems encountered above.

### 3.1. New Probes

Due to the feeding characteristics of the rectangular waveguide structure, most of the energy of the feed system is concentrated in the middle of the waveguide. When the probe is inserted into the waveguide, the electromagnetic field in the waveguide changes greatly due to the cutting of the electric field in the waveguide by the probe. Because the waveguide used can only transmit  $TE_{10}$  mode in the operating frequency, the energy is cut off at the insertion and exit of the probe, and most of the energy is reflected and fed into the inlet. The electric field distribution of the feed system at this time is shown in Fig. 5(a), which obviously affects the subsequent coupling of the probe. For this reason, the waveguide wall embedded probe is considered, whose structure is shown in Fig. 6. After using this probe form, the influence of probe addition on electromagnetic energy transmission is significantly reduced, as shown in Fig. 5(b). At this time, most of the energy can be normally transmitted along the feeding system to ensure the energy coupling of subsequent units. The influence of the probe's deviation from the center of the feeding system on its reflection and coupling is simulated and analyzed. When the probe gradually deviates from the center of the feeding waveguide in the manner shown in Fig. 7, the change in the coupling amount and reflection is shown in Fig. 8.

When the probe is deviated from the center of the waveguide, the energy at the position of the probe is gradually reduced, so that its interference with the energy transmission in the rectangular waveguide is gradually reduced, thereby effectively suppressing the influence of the probe insertion on the waveguide. The coupling amount of the probe is mainly related to the size and shape of the coaxial output port. When the probe offset distance is small, the coaxial change of the probe output is not

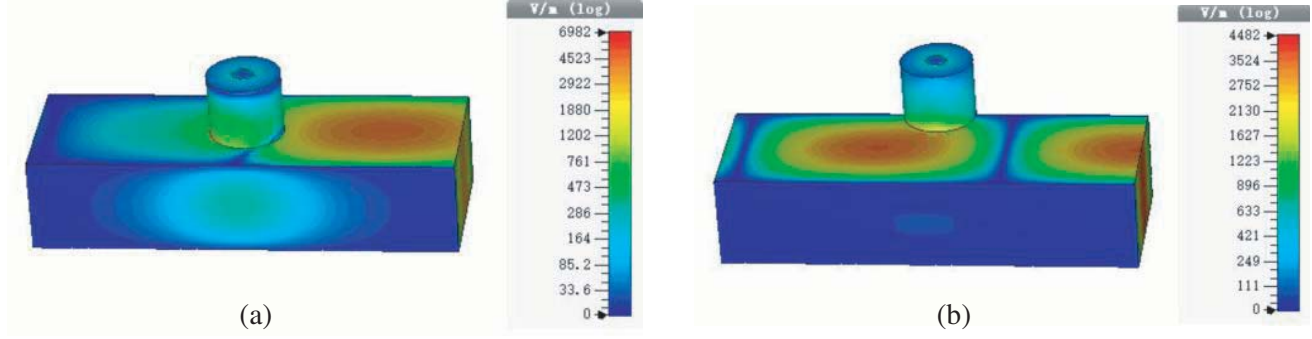


**Figure 5.** Effect of probe position on electric field. (a) Probe at center of waveguide. (b) Probe embedded the waveguide.

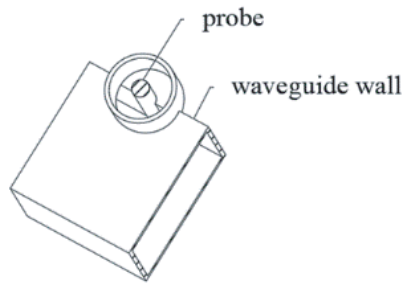


**Figure 6.** Structure of waveguide wall embedded probe.

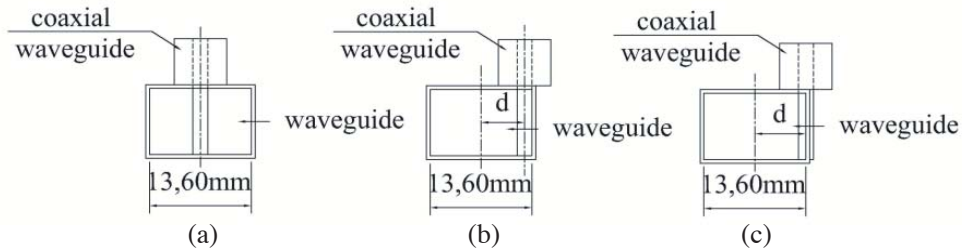


**Figure 7.** Structure of LLHS. (a) Probe at center of waveguide. (b) Probe at side of waveguide. (c) Probe embedded the waveguide.

large, so the overall coupling change is not large. When the probe is closer to the waveguide wall, the coupling ability is greatly affected due to the structural asymmetry of the output coaxial port. This problem was alleviated after the probe was further embedded in the waveguide wall.

Based on the above probes, two new kinds of probe are obtained by combining the waveguide wall embedded probe structure with other probe structures, as shown in Fig. 9. Through the selection and adjustment of the probe structure, the coupling amount can be greatly adjusted to facilitate the subsequent design of the feed system.

### 3.2. Feed System

For the LLHA, the coupling amount of each probe should be  $\sqrt{1/80} \approx 0.112$ . Because the electromagnetic energy in the long linear array feed system gradually decreases during the probe coupling process, the coupling energy of each output port can be expressed as

$$P_n = \frac{1}{81 - n} P_{re} \tag{1}$$

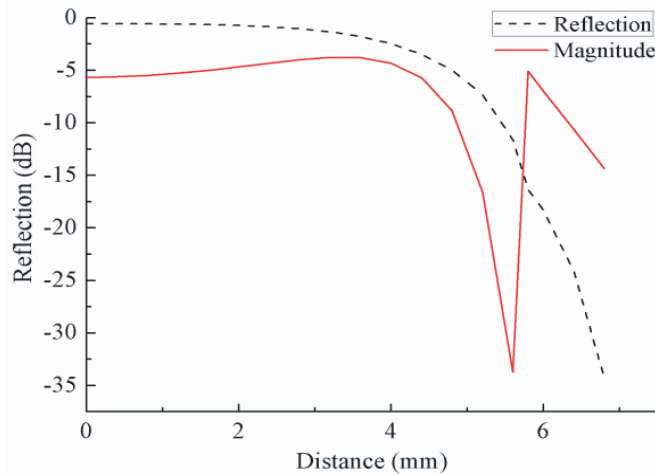


**Figure 8.** Reflection and coupling of probe offset in different distance.

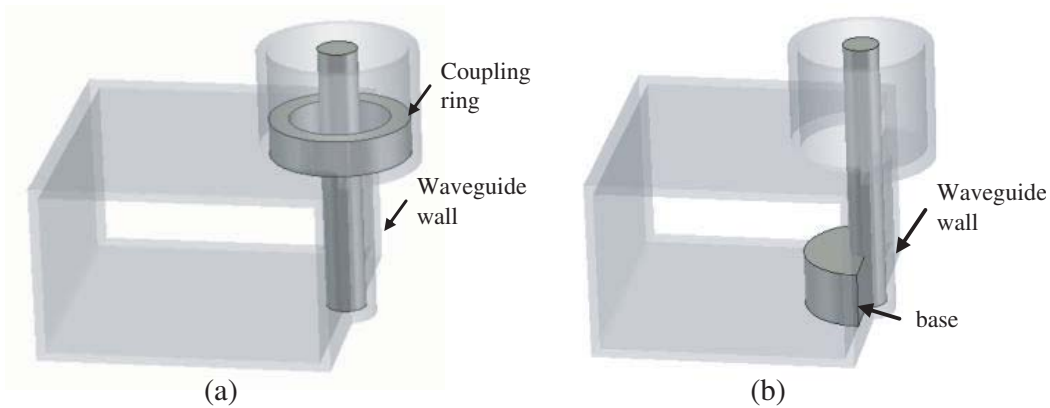


**Figure 9.** Structure of two kinds of probe. (a) Ring probe. (b) Cylindrical base probe.

where  $n$  is the  $n$ -th unit starting from the feed port,  $P_{re}$  the energy remaining when reaching the unit, and  $P_n$  the energy coupled by the unit. The relationship between the coupling amount of the two probes and the parameters proposed above is simulated, and the relationship between the coupling amount and parameters of the two probes is shown in Fig. 10.

The theoretical coupling amount of each probe output port is obtained by Equation (1). The results are compared with the simulation results of Fig. 11 to select the parameters of each unit probe. The selected probe parameters are shown in Table 2 and Table 3.

Generally, a linear array uses a load matching structure to process the remaining energy at the end of the feeding system, which results in a waste of energy by the feed system. Without load, the electromagnetic energy transmitted to the end of the waveguide will form a standing wave, which will adversely affect the reflection of the feed system and reduce the overall power capacity of the system. In order to avoid waste of energy and avoid the formation of standing waves, this paper proposes to adopt a waveguide-coaxial conversion structure as shown in Fig. 12 for sealing. The parameters of the conversion structure are optimized by simulation, and the structure can couple most of the energy transmitted to the end of the feeding system to the end radiation unit for radiation. The parameters of the transformation structure are shown in Table 4.

Finally, the overall structure of the obtained feed system is shown in Fig. 10. Considering the effect of the array antenna spacing on the grating lobe, the antenna unit spacing is selected to be 15.6 mm, and the inner and outer axial distributions of the feeding coaxial are 1 mm and 3.5 mm. The total length of the feed system is 1256.4 mm. A ring-shaped probe that suppresses the coupling amount is used in

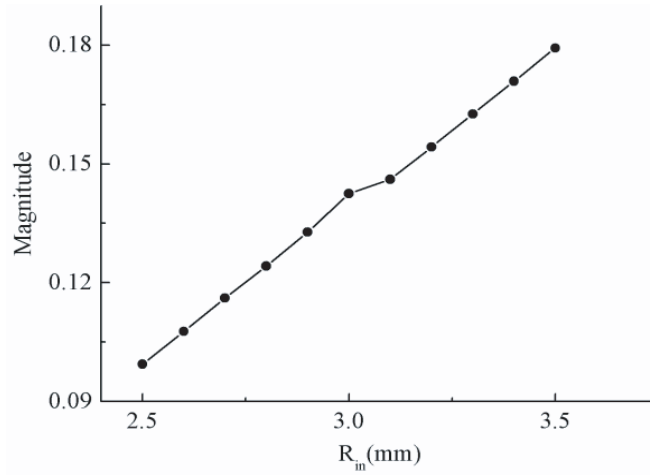


Figure 10. Relation of  $r_{in}$  and coupling magnitude.

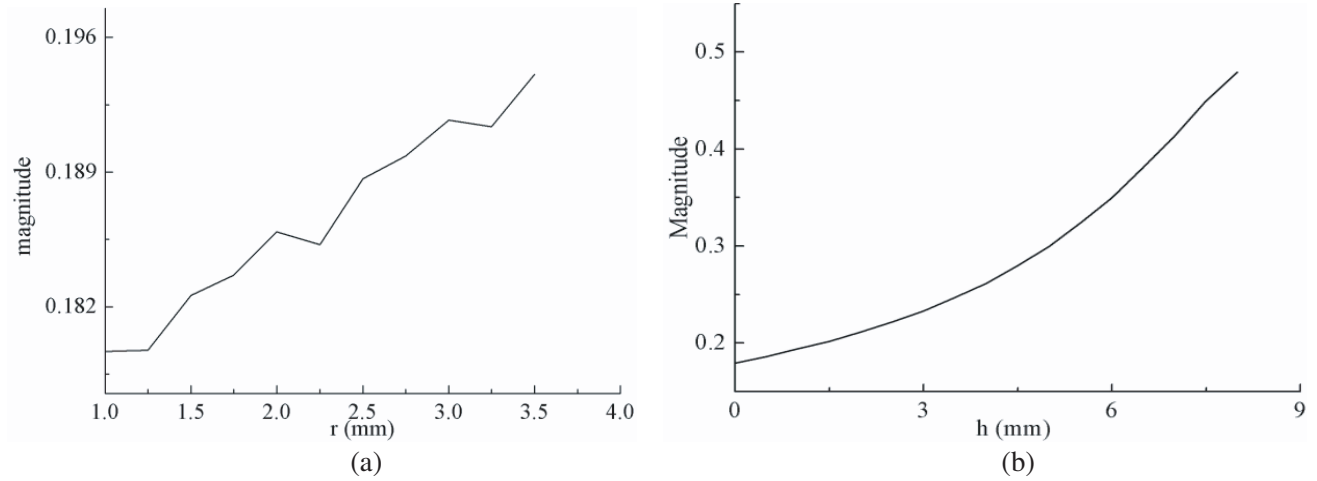


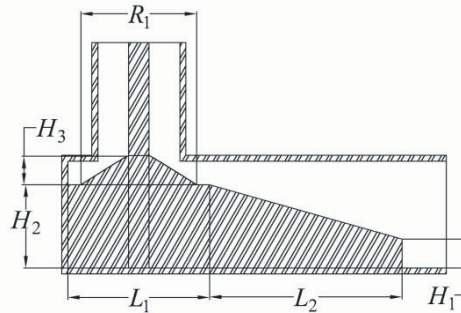
Figure 11. Coupling magnitudes of cylindrical base probe. (a) Coupling magnitudes of probe with different  $r$ . (b) Coupling magnitudes of probe with different  $h$ .

Table 2. Size of each ring probe (unit: mm).

$i$	$R_{in_i}$										
1	2.55	10	2.65	19	2.75	28	2.85	37	3.00	46	3.20
2	2.55	11	5.65	20	2.75	29	2.85	38	3.05	47	3.25
3	2.55	12	2.65	21	2.75	30	2.90	39	3.05	48	3.25
4	2.60	13	2.65	22	2.80	31	2.90	40	3.10	49	3.30
5	2.60	14	2.70	23	2.80	32	2.95	41	3.10	50	3.35
6	2.60	15	2.70	24	2.80	33	2.95	42	3.15	51	3.35
7	2.60	16	2.70	25	2.85	34	2.95	43	3.15	52	3.40
8	2.60	17	2.70	26	2.85	35	3.00	44	3.15	53	3.40
9	2.65	18	2.75	27	2.85	36	3.00	45	3.20	54	3.45

**Table 3.** Size of each cylindrical base probe.

<i>i</i>	<i>h</i>	<i>r</i>									
55	0.50	2.00	62	2.00	3.50	69	4.20	3.50	76	6.60	3.50
56	0.50	2.50	63	2.50	3.50	70	4.60	3.50	77	7.50	3.50
57	0.50	3.50	64	2.50	3.50	71	5.00	3.50	78	7.50	3.50
58	1.00	3.50	65	3.00	3.50	72	5.30	3.50	79	7.50	3.50
59	1.00	3.50	66	3.50	3.50	73	5.70	3.50	-	-	-
60	1.50	3.50	67	3.50	3.50	74	5.90	3.50	-	-	-
61	2.00	3.50	68	4.00	3.50	75	6.50	3.50	-	-	-



**Figure 12.** Structure of waveguide-coaxial adapter.

**Table 4.** Waveguide-coaxial size.

PARAMETERS	<i>h1</i>	<i>l1</i>	<i>h2</i>	<i>l2</i>	<i>h3</i>	<i>r1</i>
VALUES (MM)	2.420	12.000	7.000	16.260	2.400	4.915

the front section of the feed system, and a cylindrical base probe that can increase the coupling amount is used in the rear section. The end is sealed with a rectangular waveguide-coaxial structure. The coupling and reflection characteristics of the obtained feed system are shown in Fig. 13, and the phases of the coupling ports of feed system at 12.5 GHz are shown in Table 5. It can be seen from Fig. 14 that the unit probe coupling amounts of the feeding system are approximately equal at 12.5 GHz, and the reflection coefficient is small. It can be seen from Table 4 that at 12.5 GHz, the phases of the coupling ports are approximately uniformly distributed.

#### 4. SIMULATION AND EXPERIMENT

Combine the array model with the standard waveguide conversion structure and the coaxial-waveguide conversion structure to obtain the overall structure model for testing. The processed antenna is shown in Fig. 15.

The experiment draws feed support from a network analyzer and a microwave power amplifier of +23 dBm, and some common characteristics have been verified, such as VSWR, radiation pattern, gain, and AR. It can be read from the curves of Fig. 16 that the measured reflection coefficient agrees with the designed. Obviously, the reflection coefficient is lower than -16.91 dB between 12 and 13 GHz, while at center frequency, the reflection coefficient is -16.91 dB. The reflection coefficient gets worse far away from the center frequency, and it might be strongly ascribed to the slight errors in probe processing. The radiation patterns at 12.5 GHz are depicted in Fig. 17. The 3 dB widths of the measured and

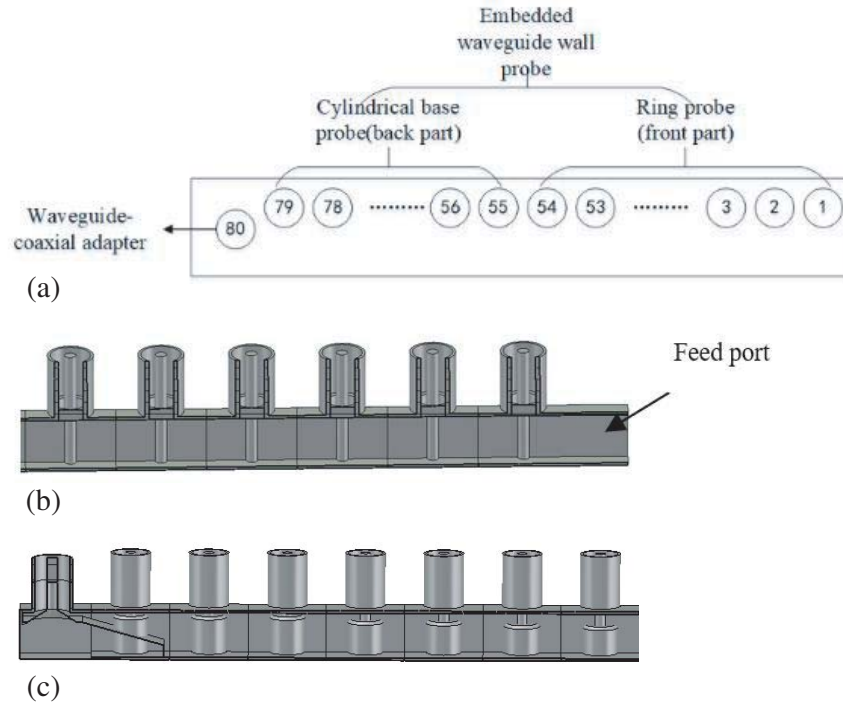


**Figure 13.** Graphs of feed system. (a) Layout of the probes. (b) Front part of feed system. (c) Back part of feed system.

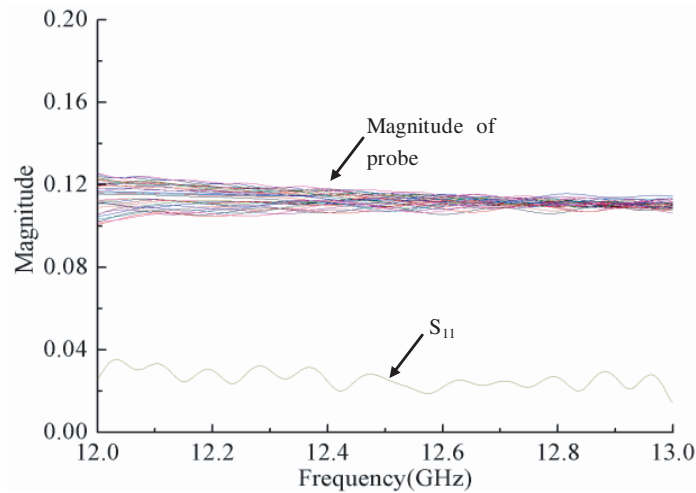


**Figure 14.** Reflection curves and coupling curves of feed system.

designed main-lobes are nearly the same, whereas the side-lobes are not. Because of the ohm losses and processing error, the measured gain is only 25.2 dB, which is 0.9 dB less than the designed value. The 3 dB width on the elevation plane is 69 deg, and the 3 dB width on the azimuth plane is 1.1 deg, which is not much different from the simulation results. The simulation AR results are plotted in Fig. 18, and the AR value measured is 2.31 dB at  $\theta = 0^\circ$ , which is larger than the theoretical 1.81 dB, but it can still realize circular polarization near  $\theta = 0^\circ$ . This is mainly caused by the error in the phase adjustment of the element antennas.

The  $E$ -field distribution inside the LLHS is shown in Fig. 19. As can be seen, the maximum  $E$ -field on the array antenna is 5012 V/m when the input power is 0.5 W, while the electric field concentration

**Table 5.** Phases of the coupling ports at 12.5 GHz (unit: °).

<i>i</i>	phase										
1	65.13	15	350.94	29	269.94	43	179.60	57	72.24	71	38.22
2	317.06	16	242.68	30	161.29	44	68.47	58	324.04	72	291.17
3	209.67	17	134.29	31	52.00	45	319.45	59	216.10	73	195.7
4	100.81	18	29.66	32	302.62	46	209.37	60	105.65	74	89.13
5	352.97	19	276.9	33	193.99	47	98.13	61	1.29	75	353.71
6	245.07	2	168.78	34	84.26	48	349.72	62	252.70	76	251.58
7	136.83	21	60.32	35	335.64	49	237.63	63	146.67	77	153.55
8	29.21	22	311.19	36	225.88	5	137.58	64	42.77	78	61.23
9	280.26	23	202.93	37	116.73	51	17.72	65	294.48	79	331.77
1	172.29	24	94.00	38	7.76	52	265.18	66	193.77	8	245.95
11	64.19	25	345.25	39	257.26	53	156.37	67	86.79		
12	315.91	26	236.25	4	148.50	54	44.30	68	344.72		
13	208.07	27	127.55	41	38.49	55	292.71	69	241.66		
14	99.06	28	19.20	42	288.09	56	184.38	7	136.69		



**Figure 15.** The photograph of the fabricated antenna.

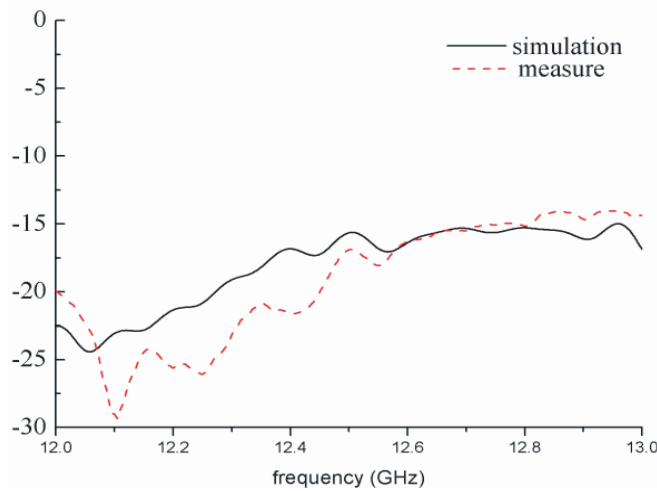


**Figure 16.** Simulation and measure reflection of the proposed antenna.

mainly appears near the No. 65 probe of the feed system. According to the Kilpatrick rule

$$f = 1.643E^2 e^{-8.5/E} \tag{2}$$

where  $f$  is the working frequency of the antenna, and the unit is MHz;  $E$  is the vacuum breakdown field strength at this frequency, and the unit is MV/m. According to the above formula, it can be calculated that the breakdown field strength of vacuum at 12.5 GHz is 913 MV/m. Use the power capacity ratio

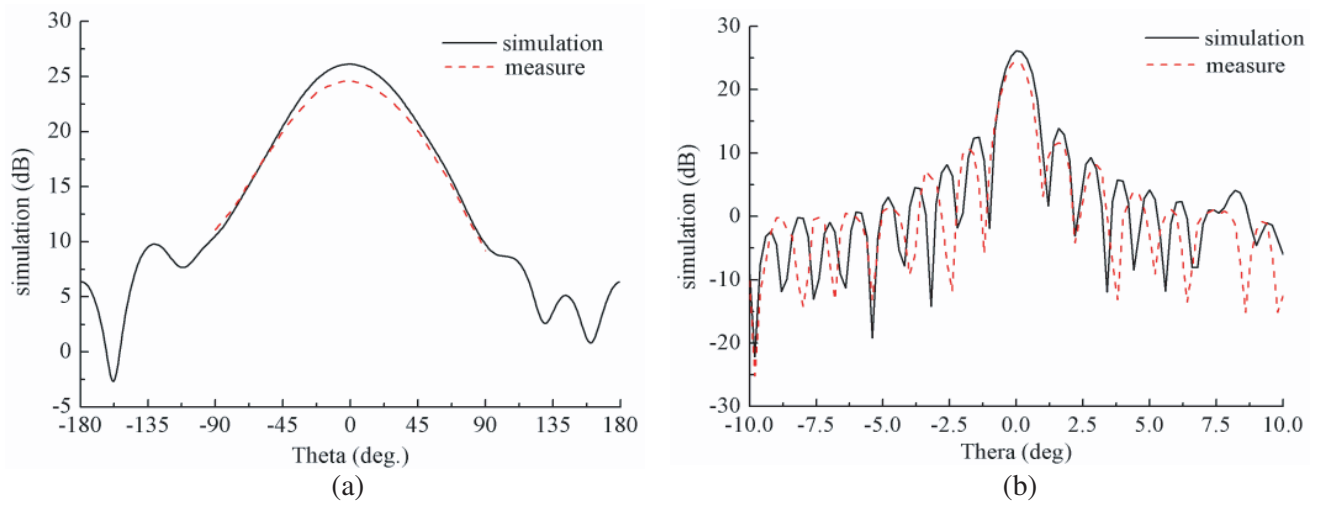


Figure 17. Simulated and measure radiation patterns of the proposed antenna.

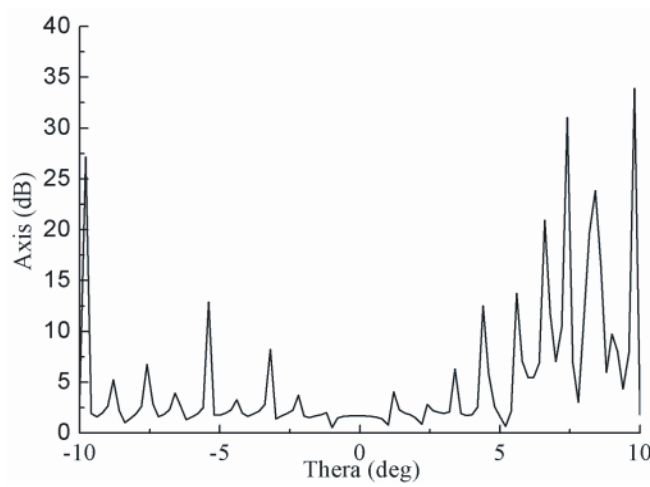


Figure 18. Simulation of axial ratio of antenna.

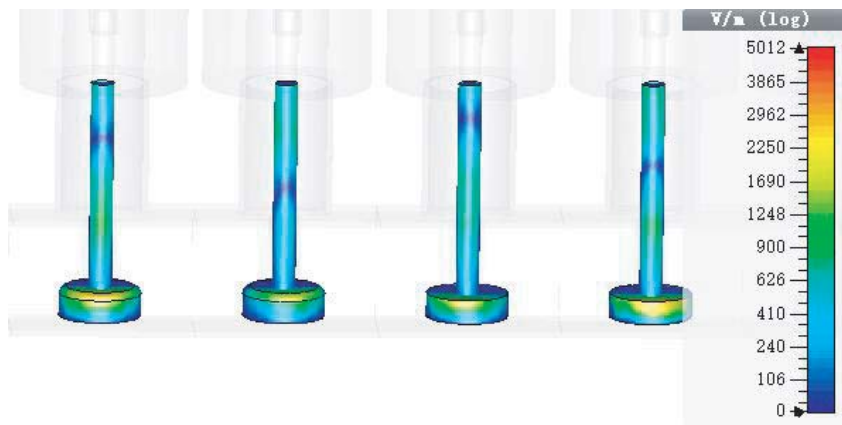


Figure 19. Electric field of the array antenna.

formula

$$P_{\max} = \frac{P_{in} E_{\max}^2}{E^2} \quad (3)$$

where  $P_{\max}$  is the system power capacity,  $P_{in}$  the simulated input power,  $E$  the input field strength corresponding to  $P_{in}$ , and  $E_{\max}$  the breakdown field strength. It can be calculated that the power capacity of the current antenna array is 166 MW.

## 5. CONCLUSION

In this paper, a long linear helical subarray (LLHA) for a high-power conformal antenna array is proposed. By using a long linear array structure, the conformal design of a cylindrical antenna can be realized. An embedded probe structure is proposed to realize equal amplitude in-phase feed of cell antenna under the condition of flat waveguide feed. The central frequency reflection of the subarray is  $-16.9$  dB, and the gain is about  $25.2$  dB, and the power capacity is 166 MW. While retaining the advantages of high-power spiral array antennas such as high gain and high power capacity, the antenna greatly reduces the narrow side size of the antenna, making it more suitable for conformal antenna arrays and better adapting to cylindrically shaped array needs, which fills the blank of high-power helical array antenna in the field of high power conformal array antenna.

## ACKNOWLEDGMENT

This work was supported by Sichuan Science and Technology Program (2018GZ0531, 2018GZ0532, 2019YFG0420) and the Fundamental Research Funds for the Central Universities (2018GF09).

## REFERENCES

1. Wen, J., D.-B. Chen, D. Wang, and F. Qin, "Preliminary experimental research on Ku-band MILO," *IEEE Transactions on Plasma Science*, Vol. 41, No. 9, 2501–2505, Sep. 2013.
2. Nallasamy, V., et al., "Advances and present trends in magnetically insulated line oscillator," *Journal of Electromagnetic Waves and Applications*, Vol. 31, No. 17, 1864–1874, 2017.
3. Guo, L., W. Huang, C. Chang, et al., "Studies of a leaky-wave phased array antenna for high-power microwave applications," *IEEE Transactions on Plasma Science*, Vol. 44, No. 10, 2366–2375, 2016.
4. Pottier, S. B., F. Hamm, D. Jousse, P. Sirot, F. T. Talom, and R. Vézinet, "High pulsed power compact antenna for high-power microwaves applications," *IEEE Transactions on Plasma Science*, Vol. 42, No. 6, 1515–1521, Jun. 2014.
5. Zhang, H. Y., F. S. Zhang, and F. Zhang, "A novel high-gain cavity slot antenna based on polarization twist reflector for high power microwave applications," *Progress In Electromagnetics Research C*, Vol. 76, 23–31, 2017.
6. Zhao, X. and C. Yuan, "All-metal beam steering lens antenna for high power microwave applications," *IEEE Transactions on Antennas and Propagation*, Vol. 65, No. 12, 7340–7344, Dec. 2017.
7. Lawrance, J. E. and C. G. Christodoulou, "A high-power microwave zoom antenna with metal-plate lenses," *IEEE Transactions on Antennas and Propagation*, Vol. 64, No. 8, 3380–3389, Aug. 2015.
8. Li, X. and Q. Liu, "A GW level high power radial helical antenna," *IEEE Transactions on Antennas and Propagation*, Vol. 56, No. 9, 2943–2948, Sept. 2008.
9. Li, X. Q., Q. X. Liu, and J. Q. Zhang, "High power 12-element triangular-grid rectangular radial line helical array antenna," *Progress In Electromagnetics Research C*, Vol. 55, 17–24, 2014.
10. Peng, S. and C. Yuan, "Linearly polarised radial line slot antenna for high-power microwave application," *IET Microwave Antennas & Propagation*, Vol. 11, No. 5, 680–684, Apr. 2017.
11. Lee, J. M. and J. M. Woo, "Design of array synthesis horn antenna for high power microwave applications," *Progress In Electromagnetics Research*, 1196–1198, 2012.

12. He, Q. Q. and B. Z. Wang, "Radiation patterns synthesis for a conformal dipole antenna array," *Progress In Electromagnetics Research*, Vol. 76, 327–340, 2007.
13. Xu, H. and B. Zhang, "Wide solid angle beam-switching conical conformal array antenna with high gain for 5G applications," *IEEE Antennas and Wireless Propagation Letters*, Vol. 17, No. 12, 2304–2308, Dec. 2018.
14. Singh, P. K. and J. Saini, "Reconfigurable microstrip antennas conformal to cylindrical surface," *Progress In Electromagnetics Research Letters*, Vol. 72, 119–126, 2018.
15. Braaten, B. D. and S. Roy, "A self-adapting flexible (SELFLEX) antenna array for changing conformal surface applications," *IEEE Transactions on Antennas and Propagation*, Vol. 61, No. 2, 655–665, Feb. 2013.
16. Nechaev, Y. and I. Peshkov, "Evaluation and minimization of Cramer-Rao bound for conformal antenna arrays with directional emitters for DOA-estimation," *Progress In Electromagnetics Research C*, Vol. 90, 139–154, 2019.
17. Huang, J. Q., D. Lei, C. Jiang, et al., "Novel circularly polarized SIW cavity-backed antenna with wide CP beamwidth by using dual orthogonal slot split rings," *Progress In Electromagnetics Research C*, Vol. 73, 97–104, 2017.
18. Sahnoun, N., I. Messaoudene, T. A. Denidni, et al., "Integrated flexible UWB/NB antenna conformed on a cylindrical surface," *Progress In Electromagnetics Research Letters*, Vol. 55, 121–128, 2015.
19. Sam, K. U. and P. Abdulla, "Truncated circular microstrip ultra wideband antenna exhibiting wideband circular polarization," *Progress In Electromagnetics Research C*, Vol. 99, 111–122, 2020.
20. Wu, Y. F. and Y. J. Cheng, "Conical conformal shaped-beam substrate integrated waveguide slot array antenna with conical-to-cylindrical transition," *IEEE Transactions on Antennas and Propagation*, Vol. 65, No. 8, 4048–4056, Aug. 2017.
21. Singh, P. K. and J. Saini, "Effect of varying curvature and inter element spacing on dielectric coated conformal microstrip antenna array," *Progress In Electromagnetics Research M*, Vol. 58, 11–19, 2017.
22. Liang, Y. and J. Zhang, "High-power dual-branch helical antenna," *IEEE Antennas and Wireless Propagation Letters*, Vol. 17, No. 3, 472–475, Mar. 2018.